AIAA Meeting Papers on Disc, January 1997
A9715500, AIAA Paper 97-0439

Onset of the spiral mode of vortex breakdown

Andrew W. Cary
Michigan Univ., Ann Arbor

David L. Darmofal
Michigan Univ., Ann Arbor

Kenneth G. Powell
Michigan Univ., Ann Arbor

AIAA, Aerospace Sciences Meeting & Exhibit, 35th, Reno, NV, Jan. 6-9, 1997

The 3D nature of vortex breakdown, while widely recognized, has seldom been included in the analytical investigations and, until recently, the numerical simulations of this phenomenon. The principle asymmetric effects are examined by considering the impact that a weak perturbation has on an axisymmetric vortex. It is demonstrated that large axisymmetric strain rates are required for a nonaxisymmetric perturbation to grow. Simulations bear out this fact by showing significant asymmetric behavior only after a critical swirl is exceeded which leads to breakdown in an axisymmetric flow. This result supports previous investigations which predict breakdown for an axisymmetric flow, despite their inability to fully capture the complexity of the breakdown topology. Furthermore, this finding indicates that vortex breakdown may be a predominantly axisymmetric occurrence which is complicated by 3D effects. (Author)

Onset of the Spiral Mode of Vortex Breakdown

Andrew W. Cary* David L. Darmofal† Kenneth G. Powell‡
University of Michigan, Ann Arbor, Michigan 48105

Abstract

The three-dimensional nature of vortex breakdown, while widely recognized, has seldom been included in the analytical investigations and, until recently, the numerical simulations of this phenomenon. The principle asymmetric effects are examined by considering the impact that a weak perturbation has on an axisymmetric vortex. It is demonstrated that large axisymmetric strain rates are required for a non-axisymmetric perturbation to grow. Simulations bear out this fact by showing significant asymmetric behavior only after a critical swirl is exceeded which leads to breakdown in an axisymmetric flow. This result supports previous investigations which predict breakdown for an axisymmetric flow, despite their inability to fully capture the complexity of the breakdown topology. Furthermore, this finding indicates that vortex breakdown may be a predominantly axisymmetric occurrence which is complicated by three-dimensional effects.

Introduction

A wide variety of large amplitude perturbations of swirling flows have been classified as vortex breakdown since the disruption was first observed by Peckham and Atkins[1]. These different flows have been classified with flow visualization by both Sarpkaya[2] and Faler and Leibovich[3] into as many as six different types ranging from the general "bubble" and "spiral" forms to the more exotic "double helix". In general, vortex breakdown is characterized by the presence of a stagnation point in a vortex-dominated flow and a loss in the coherence of the vortex structure followed by a rapid decay into turbulence. Applications of vortex breakdown occur for both internal and external flows. The ability to predict and control the presence of vortex breakdown can lead to improved mixing in flame holders as well as more efficient and more robust aircraft wings.

While vortex breakdown has been studied and analyzed for over forty years, a theory has yet to be accepted which can describe both its formation and its evolution. Early efforts to understand this phenomenon focused on wave theories, hydrodynamic instability, and a separation analogy[4]. The approaches using wave theories postulated either an abrupt transition similar to a hydraulic jump[5, 6] or an accumulation of waves which could not propagate upstream[7]. Recently, more detailed studies of vortex dynamics have yielded insight into the feedback mechanisms which lead to the formation of axisymmetric breakdown[8, 9]. Numeric simulations have indicated that the appearance of breakdown can be correlated to a transition from supercritical flows to subcritical flows[10]. It has also been demonstrated[11, 12, 13] that non-unique solutions exist for swirling flows over a range of vortex strengths and that these solutions exchange sta-

*Graduate Student, University of Michigan, Student Member AIAA.

†Professor, Department of Aerospace Engineering, Texas A & M University, Professional Member AIAA.

‡Professor, Department of Aerospace Engineering, University of Michigan, Senior Member AIAA.

bilities at a critical swirl ratio[14].

Each of these theories offer insight into facets of vortex breakdown, but none adequately describes both the occurrence and topology of breakdown. Additionally, a necessary limitation of many of the theories to date has been the assumption of axisymmetric flow. Although the bubble form of breakdown is largely axisymmetric, the internal structure has many asymmetries. The influences of the asymmetry and the alternative forms of breakdown on stability and breakdown formation have yet to be fully examined. This study attempts to fill some of this void. Additional non-axisymmetric simulations have been performed by Spall[15], Ma and Leibovich[16], Tromp and Beran[17], and Lucas[18]. This project, however, is unique by concentrating on the evolution of each of the azimuthal modes.

Approach

The flow is modeled using the unsteady, incompressible, Navier-Stokes equation written in cylindrical coordinates. This equation is Fourier-decomposed in the azimuthal direction resulting in a coupled system of partial differential equations. Specifically, the flow field variables are represented by the truncated Fourier series

$$f(r,\theta,z,t) = f_0(r,z,t) + \sum_{n=1}^{N_\theta} \left(f_n(r,z,t)e^{-\imath n\theta} + \bar{f}_n(r,z,t)e^{\imath n\theta} \right), \quad (1)$$

where (r,θ,z) specify the cylindrical coordinates and t represents time. The non-axisymmetric terms, f_n, are complex with the imaginary component representing a phase shift of 90 degrees from the real component. N_θ is the number of Fourier modes used to represent the flow and a bar over a symbol indicates its complex conjugate.

Analytic basis

The local strength of each Fourier mode can be represented by an energy-like magnitude term, $q_n = \frac{1}{2} \parallel \mathbf{u}_n - \mathbf{U}_n \parallel^2$, where $\mathbf{u}_n$ is the nth Fourier component of the velocity and $\mathbf{U}_n$ is similarly a Fourier component of a base flow. This quantity can be shown to obey an advection-diffusion equation with source terms stemming from pressure work, viscous dissipation, and interaction with other Fourier modes. In the following runs, the pressure term was insignificant compared to the other sources of q_n. While the viscous dissipation rate was of the same order as the non-linear interactions, it was highly localized about the axis.

If a smooth axisymmetric flow is weakly perturbed with an $n = 1$ disturbance of magnitude $\mathcal{O}(\epsilon)$, the quadratic nature of the non-linear interaction term indicates that the magnitude of the higher azimuthal modes will initially be $\mathcal{O}(\epsilon^n)$. This cascade in amplitude can be modified if the strain is locally increased or if a radial mode is triggered with a significant growth factor. Using this amplitude information, the Fourier decomposed momentum equation can be linearized to find that the non-axisymmetric disturbance has a feedback term with a gain which is roughly proportional to the strain rate in the base flow. This potential for feedback indicates that rapid growth of non-axisymmetric modes can be triggered by an increase in the local strain, such as occurs near the stagnation point at the leading edge of a "bubble" breakdown.

To study the global interaction between the various modes, the integral over the volume of the velocity's Fourier-mode magnitude, q_n, will be evaluated throughout a flow field.

$$Q_n = \int_0^L \int_0^{R(z)} q_n r \, dr \, dz \quad (2)$$

This quantity gives an indication of the relative significance of each azimuthal mode in the flow. Integrating the differential equation for q_n over space leads to an equation for $Q_n(t)$. Using Gauss's theorem, the changes in Q_n can be identified with changes along the boundary and volumetric changes. Convection of q_n, pressure work, and viscous stress are boundary effects, while viscous dissipation, and a non-linear interaction with other Fourier velocity modes are the

volume sources.

Numeric scheme

The rotational form of the unsteady, Fourier-decomposed, incompressible Navier-Stokes equations are solved in primitive variables using an Orszag-Kells operator splitting[19] scheme to break the equation into an advection step, a pressure update which forces mass conservation, and a viscous correction:

$$\begin{aligned}
\frac{\mathbf{u}^{n+1/3}-\mathbf{u}^{n}}{\Delta t} &= \frac{3}{2}\mathbf{u}^{n}\times\omega^{n}-\frac{1}{2}\mathbf{u}^{n-1}\times\omega^{n-1} \\
\frac{\mathbf{u}^{n+2/3}-\mathbf{u}^{n+1/3}}{\Delta t} &= -\nabla H^{n+1}, \text{ where} \qquad (3) \\
& \quad \Delta t\nabla^{2}H^{n+1}=\nabla\cdot\mathbf{u}^{n+1/3} \\
\frac{\mathbf{u}^{n+1}-\mathbf{u}^{n+2/3}}{\Delta t} &= \frac{\gamma}{Re}\nabla^{2}\mathbf{u}^{n+1}+ \\
& \quad \frac{1-\gamma}{Re}\nabla^{2}\mathbf{u}^{n+2/3}.
\end{aligned}$$

In these equations, $\mathbf{u}$ is the velocity and ω is the vorticity. This numerical approach is second-order accurate in time. Radial derivatives are evaluated using Chebyschev collocation and axial derivatives are obtained from finite-differences. The convolution sums arising from the Fourier-decomposition are explicitly calculated to avoid aliasing. The Laplacian operator appearing in the pressure Poisson equation and the viscous correction is implicitly inverted using a block Thomas algorithm. In order to decouple the non-axisymmetric radial and azimuthal velocity system in the viscosity correction, the linear combinations $(u_n \pm iv_n)^{n+1}$ were solved for in the Helmholtz equation. This leads to two decoupled sets of equations which can then be separated to find the radial and azimuthal velocities.

The sinusoidal nozzle geometry used by previous investigators[12, 9] is also adopted here. This geometry creates a favorable pressure gradient which prevents the breakdown from propagating upstream of the nozzle and affecting the inlet boundary condition. To remove wall boundary layer separation from this study, the velocity was allowed to slip along the nozzle, leading to the outer boundary representing a rigid axisymmetric streamtube. To decrease the impact on accuracy of operator splitting in the interior of the domain, a higher-order pressure boundary condition is applied at this boundary[20]. The outflow is parabolized by neglecting the second derivative in the axial direction. This boundary condition is justified by the flow's tendency to return to a supercritical state due to viscous effects. The axis boundary conditions are obtained from constraints imposed as a consequence of the Fourier decomposition. Finally, the inlet velocity profile is specified to provide control over the flow entering the domain.

Results from this code have been favorably compared to both experimental and analytic results. Detailed comparisons have been made to AI, an axisymmetric, finite-volume code written by Darmofal[9], which uses a streamfunction-vorticity formulation. The solutions from these two codes agree very well in both spatial and temporal variations as illustrated in Figure 1. This figure compares the streamfunction contours in the vicinity of a breakdown bubble. The upper half of the flow is an AI calculation on a 30×300 grid, while the lower half is the result of the present code calculated on a 18×150 grid. The slight waviness in the contours is largely due to a combination of integrating the velocity to find the streamfunction and the use of bi-linear interpolation in obtaining the contours rather than spectral interpolation.

Results

A moderate core Reynolds number of 500 was used for the following runs, eliminating the need for a turbulence model. The inlet had a radius of 2 core radii and converged to 90% of this value before growing to a test section of 2.2 core radii. The grid and geometry are depicted in Figure 2 and used 17 collocation points in the radial direction and 100 points in the axial direction. Grid resolution studies indicate that this grid is sufficient for swirl ratios up to about 1.3. The Chebyschev coefficients in the radial direction showed an amplitude decrease of about five orders of magnitude for a solution with break-

down, indicating adequate resolution.

The axisymmetric flows used as base solutions were obtained by beginning with a non-swirling flow and gradually increasing the circulation by a small amount. The flow was allowed to converge and the process was repeated to obtain a series of solutions ranging from a non-swirling case to flows exhibiting breakdown. A non-dimensional circulation, $\Gamma/\delta W_\infty$, is used to parameterize the solutions, where Γ is the far-field circulation, δ is the core radius, and W_∞ is the free-stream axial velocity. Steady-state axisymmetric breakdown is predicted to occur for swirl ratios greater than the critical swirl of about 1.14.

Perturbation dependency on base flow

The axisymmetric base flows were perturbed at the inlet by an $n = 1$ axial velocity disturbance with an amplitude of 1% of the inlet's axial velocity. The radial distribution of the disturbance, $r^2 \exp(-12r^2)$, is similar in shape to an unstable ring mode. After growing linearly in time to its maximum strength, the disturbance's magnitude was held constant. Both $n = 1$ and $n = 2$ modes were used for these simulations.

For non-breakdown base flows, the perturbation was convected about the axis and decayed with virtually no effect on the base flow. This is exhibited by using Q_0 to measure the axisymmetric perturbation from the base flow. For swirl ratios less than the critical ratio for breakdown, Q_0 is $\mathcal{O}(10^{-6})$. Similarly, the effects of the perturbation does not significantly stimulate the $n = 2$ modes until the critical swirl is reached. For non-breakdown swirl ratios, Q_1 is $\mathcal{O}(10^{-4})$ and decays slightly with increasing swirl ratio as a consequence of increased dissipation as it is convected about the axis at faster and faster rates.

As the critical swirl is exceeded, the passive nature of the disturbance changes drastically. Not only does the $n = 1$ disturbance grow, but also its effect on the axisymmetric and $n = 2$ mode becomes dramatic. Figure 3 depicts the variations in Q_1 and the rapid increase as the critical swirl is surpassed is evident. As the critical swirl is exceeded, Q_1 jumps by nearly two orders of magnitude, reflecting the larger non-axisymmetric velocities which are present.

Perturbation flow evolution

As indicated in the previous section, perturbing a flow with axisymmetric breakdown leads to considerably different flow solutions than pre-breakdown flows. Figure 5 displays streaklines from an axisymmetric base flow with breakdown (swirl ratio = 1.2). These streaklines originate in a circle with a radius of about 2% of the core radius and centered on the axis. Note that the same starting points will be used for all subsequent streakline figures. For the base flow, the lines clearly indicate both the axisymmetric recirculation region and the stagnation point on the axis. Figure 4 depicts the variations of Q_0, Q_1, and Q_2 with time after perturbing the axisymmetric flow with a 1% non-axisymmetric disturbance. As before, the axisymmetric solution prior to perturbation is used as the base flow for obtaining Q_i. The initial growth of Q_1 is a result of increasing the amplitude at the inlet. This is followed by the basic convection of the disturbance through the flow domain. Until about $t^* = tW_\infty/\delta = 25$, when the perturbation is beginning to affect the breakdown, there is little impact on Q_0 or Q_2 and the flow shows only weak non-axisymmetric effects. However, the variations in these modes grow rapidly beyond this point.

Figure 6 through Figure 13 depict the evolution of the flow solution in additional increments of 25 non-dimensional time units. Both streakline visualization and maps of q_1 and its source term due to non-linear mode interaction are depicted. For this solution, pressure work has no significant effect and viscous dissipation is concentrated near the axis. At $t^* = 50$, the non-axisymmetric magnitudes have nearly peaked, but there is still a stagnation point on the axis. The streaklines indicate the turning from the axis and the beginning of a spiral as the vortex core is disturbed from the axis. By $t^* = 75$, the stagna-

tion point has moved off the axis and the spiral is becoming more pronounced. The sharp turn has smoothed a bit and the asymmetry is evident in the solution at $t^* = 100$. As the structure precesses about the axis, the stagnation point periodically approaches the axis and increases the turning of the core away from the axis. This is illustrated in the streaklines at $t^* = 125$ which depicts a more rapid flow turning than those at $t^* = 100$. From this point on, the structure of the solution changes little, but it continues to precess. Unlike the cases with a lower base swirl ratio, this solution did not reach a steady-state, but this quasi-steady solution with precession appears to be the end result. This observation is substantiated by the lack of variation in Q_i.

The contour plots depict the variations of q_1 and its principle source term as a function of space and time. The contours of q_1 are spaced with a difference of 0.02 between levels, while the contours of the Fourier-mode interaction source are spaced with a difference of 0.001. Gray contours indicate sinks. At $t^* = 50$, the $n = 1$ mode is strong with a peak magnitude of about 1 and has significant strength over most of the region downstream of breakdown. Its magnitude is being pulled into other modes inside the vortex core, but is being reinforced by other modes outside of the core. As time progresses, more of this mode is passed into its harmonic, the $n = 2$ mode. Additionally, the interaction source begins to focus itself into paired regions of sources and sinks as the vortex core is pulled from the axis. By $t^* = 125$, when the stagnation point is closer to the axis, the $n = 1$ mode is dominant near where the core turns away from the axis, as it must be to effect this change. Additionally, a "tail" of significant asymmetry extends downstream. The sources have aligned themselves into two paired regions. In the upstream region, the sink is near the axis, while this order is reversed downstream. Since the dominant $n = 1$ velocity component is axial, these regions represent sources of asymmetric azimuthal vorticity.

Conclusions

Three-dimensional, unsteady, numerical simulations of breakdown flows indicate that while the assumption of axisymmetry imposes a significant limitation in determining the specific structure of breakdown, it does not seem to affect the prediction of its occurrence. While more detailed work is needed to confirm this result, it is in good agreement with the experimental and analytic results which indicate that flows downstream of breakdown are linearly unstable.

The integrated velocity magnitude of each Fourier mode in the flow has also been examined. This quantity has only two volumetric source terms: viscous dissipation and non-linear interaction from other Fourier modes. The viscous dissipation term is negative definite and tends to reduce non-axisymmetric effects near the axis. The non-linear interaction term is more complicated, but represents, for weak perturbations to an axisymmetric flow, a feedback term which is proportional to the axisymmetric strain rate. This term not only pulls energy from the axisymmetric mode, but also distributes it to other harmonics.

Simulations have been performed which track this quantity and indicate that there is no significant growth in the perturbation until the critical swirl is exceeded. Base flows with lower swirl ratios lead primarily to viscous dissipation. The large strain rate, such as seen near the leading edge of an axisymmetric bubble, is necessary to reinforce the asymmetric perturbation and lead to growth.

Further work is being performed to determine the impact that the perturbation's magnitude has on its effects, as well as considering additional disturbance modes. The modifications in axisymmetric structure as swirl is increased further beyond the critical swirl will also be examined.

References

1 Peckham, D. H. and Atkinson, S. A., "Preliminary Results of Low Speed Wind Tunnel Tests on a Gothic Wing of Aspect Ratio 1.0", CP 508, Aeronautics Research Council, 16 pp., 1957.

2 Sarpkaya, T., "Vortex Breakdown in Swirling Conical Flows", *AIAA Journal* **9**(9), 1792–1799, 1971.

3 Faler, J. H. and Leibovich, S., "Disrupted States of Vortex Flow and Vortex Breakdown", *The Physics of Fluids* **20**(9), 1385–1400, 1977.

4 Hall, M. G., "Vortex Breakdown", *Annual Review of Fluid Mechanics* **4**, 195–217, 1972.

5 Benjamin, T. B., "Theory of the Vortex Breakdown Phenomenon", *Journal of Fluid Mechanics* **14**, 593–629, 1962.

6 Benjamin, T. B., "Some Developments in the Theory of Vortex Breakdown", *Journal of Fluid Mechanics* **28**, 65–84, 1967.

7 Squire, H. B., "Analysis of the "Vortex Breakdown" Phenomenon: Part I", Report 102, Aero. Dept., Imperial College, London, Also in *Miszellaneen der Angewandten Mechanik*, pp. 306–312, 1962. Berlin: Akademie-Verlag, 1960.

8 Brown, G. L. and Lopez, J. M., "Axisymmetric Vortex Breakdown. Part 2. Physical Mechanisms", *Journal of Fluid Mechanics* **221**, 553–576, 1990.

9 Darmofal, D. L., *A Study of the Mechanisms of Axisymmetric Vortex Breakdown*, PhD thesis, Massachusetts Institute of Technology, 1993.

10 Darmofal, D. L., Cary, A. W., and Powell, K. G., "Wave Propagation Characteristics of Vortical Flows in Varying-Area Pipes", AIAA 95-2307, 1995.

11 Leibovich, S. and Kribus, A., "Large-amplitude Wavetrains and Solitary Waves in Vortices", *Journal of Fluid Mechanics* **216**, 459–504, 1990.

12 Beran, P. S. and Culick, F. C., "The Role of Non-uniqueness in the Development of Vortex Breakdown in Tubes", *Journal of Fluid Mechanics* **242**, 491–527, 1992.

13 Wang, S. and Rusak, Z., "A Theory of the Axisymmetric Vortex Breakdown in a Pipe", Aeronautical Engineering Report 107, Rensselaer Polytechnic Institute, Troy, New York, 1995.

14 Wang, S. and Rusak, Z., "On the Stability of Non-Columnar Swirling Flows", Aeronautical Engineering Report 109, Rensselaer Polytechnic Institute, Troy, New York, 1995.

15 Spall, R. E. and Gatski, T. B., "Unsteady Three-Dimensional Vortex Breakdown: Visualization and Analysis", AIAA 95-2306, 1995.

16 Ma, W. and Leibovich, S., "Numerical Experiments on Vortex Breakdown", American Physics Society Division of Fluid Dynamics Annual Conference, 1994.

17 Tromp, J. C. and Beran, P. S., "Temporal Evolution of Three-Dimensional Vortex Breakdown from Steady, Axisymmetric Solutions", AIAA 95-2310, 1995.

18 Lucas, K. V. and Lele, S. K., "Numerical Investigation of Unsteady Three Dimensional Vortex Breakdown", American Physics Society Division of Fluid Dynamics Annual Conference, 1996.

19 Orszag, S. A. and Kells, L. C., "Transition to Turbulence in Plane Poiseuille and Plane Couette Flow", *Journal of Fluid Mechanics* **96**, 159–205, 1980.

20 Karniadakis, G. E., Israeli, M., and Orszag, S. A., "High-Order Splitting Methods for the Incompressible Navier-Stokes Equations", *Journal of Computational Physics* **97**, 414–443, 1991.

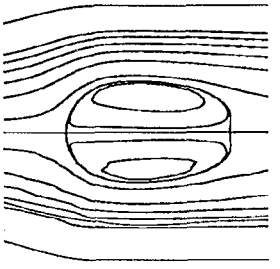

Figure 1: Comparison of axisymmetric breakdown bubble between current code (lower) and AI(upper)

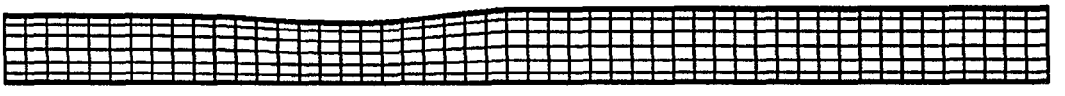

Figure 2: Computational grid and nozzle geometry (Only every other grid line drawn).

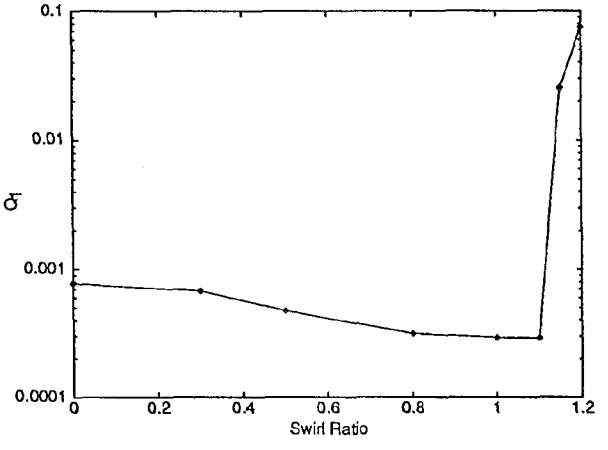

Figure 3: Steady-state $n = 1$ integrated velocity magnitude (Q_1) vs. inlet swirl ratio.

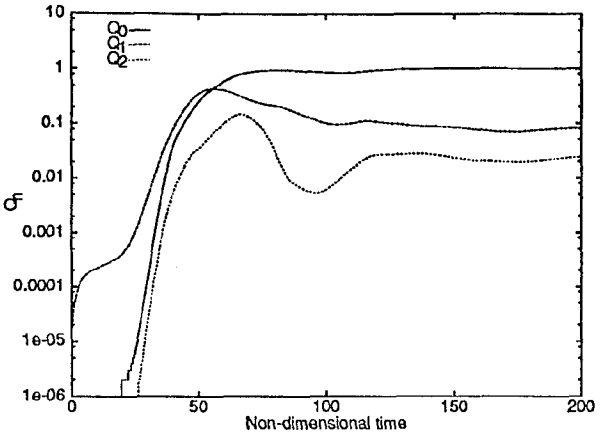

Figure 4: Development of Fourier modes with time, Swirl = 1.2.

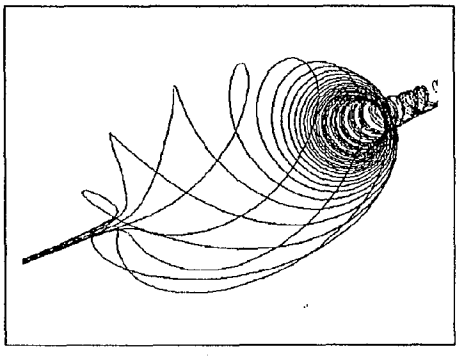

Figure 5: Streaklines for axisymmetric base flow, Swirl = 1.2.

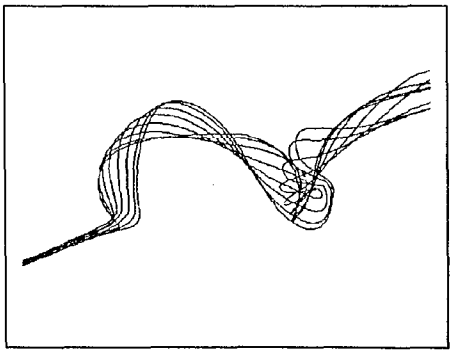

Figure 6: Streaklines for perturbed flow, Swirl = 1.2, $t^{\star} = 50$.

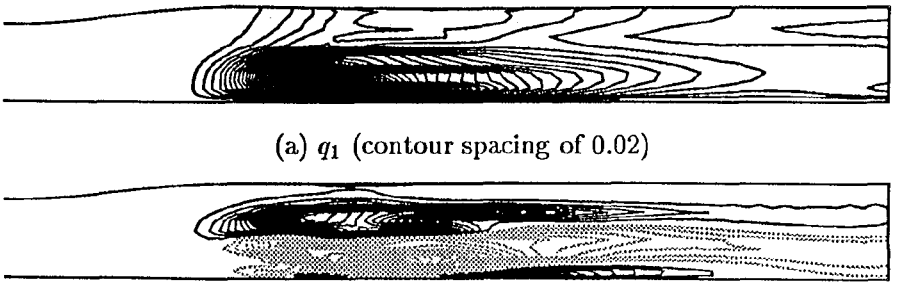

(a) q_1 (contour spacing of 0.02)

(b) Non-linear Fourier-mode interaction source (contour spacing of 0.001)

Figure 7: $n = 1$ energy map, $t^* = 50$.

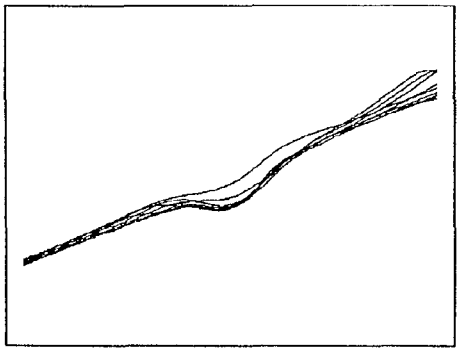

Figure 8: Streaklines for perturbed flow, Swirl = 1.2, $t^* = 75$.

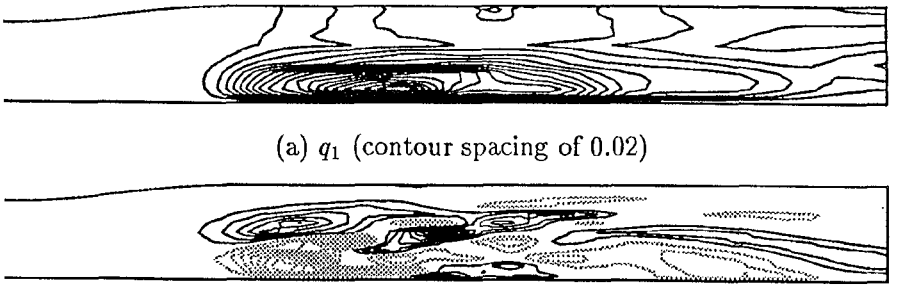

(a) q_1 (contour spacing of 0.02)

(b) Non-linear Fourier-mode interaction source (contour spacing of 0.001)

Figure 9: $n = 1$ energy map, $t^* = 75$.

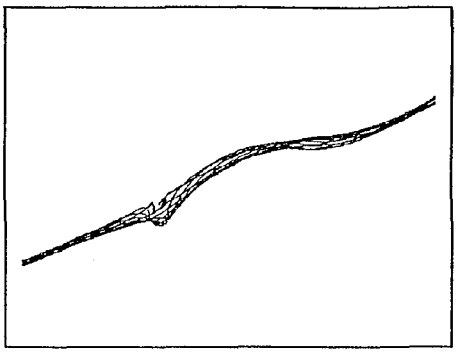

Figure 10: Streaklines for perturbed flow, Swirl = 1.2, $t^\star = 100$.

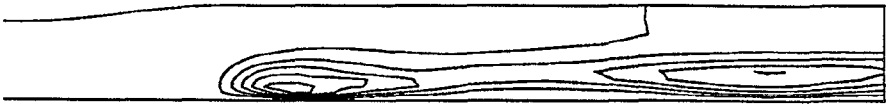

(a) q_1 (contour spacing of 0.02)

(b) Non-linear Fourier-mode interaction source (contour spacing of 0.001)

Figure 11: $n = 1$ energy map, $t^\star = 100$.

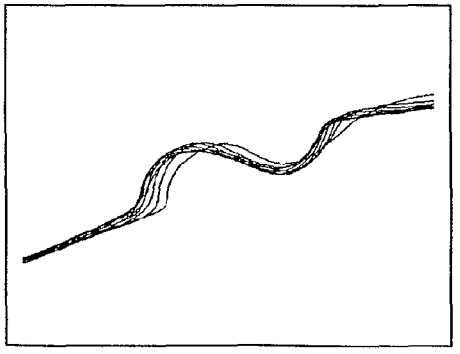

Figure 12: Streaklines for perturbed flow, Swirl = 1.2, $t^\star = 125$.

(a) q_1 (contour spacing of 0.02)

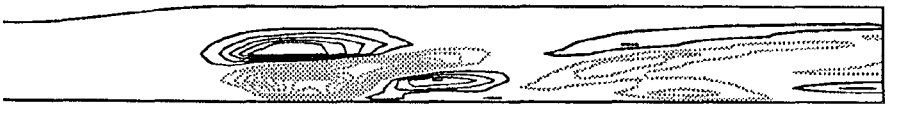

(b) Non-linear Fourier-mode interaction source (contour spacing of 0.001)

Figure 13: $n = 1$ energy map, $t^\star = 125$.